

Article

Improved Modeling of Temperature Evolution during Lung Cancer Tumor Thermal Ablation

Marwa Selmi ^{1,2} 

¹ Department of Radiological Sciences and Medical Imaging, College of Applied Medical Sciences, Majmaah University, Majmaah 11952, Saudi Arabia; m.selmi@mu.edu.sa

² Laboratory of Electronics and Microelectronics, Faculty of Science of Monastir, University of Monastir, Environment Boulevard, Monastir 5019, Tunisia

Abstract: Microwave ablation (MWA) represents one of the most powerful tools in cancer treatment. This therapeutic modality process is governed by the temperature and absorbed dose of radiation of the cell tissue. This study was performed to control the temperature effect using simulation during the MWA thermal damage of lung tumor. For this reason, a two-dimensional (2D) computational modeling generated for adaptive lung tissue was designed and analyzed using the finite element method (FEM). Different approaches, such as first-order Arrhenius rate equations, Maxwell equations, and the bioheat equation, have been used to simulate necrosis in cells. To control the heat, a proportional–integral–derivative (PID) controller was used to moderate the input microwave power source and to maintain the temperature of the target tip at a lower level of the initial temperature data. Furthermore, full cancer tissue necrosis was also evaluated by processing time and thermal damage fraction. The obtained data proved that the target tip temperature was affected by the temperature distribution and specific absorption rate (SAR). However, a specific treatment period of tumor ablation is required to control and decrease the damage of surrounding healthy tissue to ensure a safe operation without any risk.

Keywords: lung tumor; microwave ablation; PID controller; finite element method



Citation: Selmi, M. Improved Modeling of Temperature Evolution during Lung Cancer Tumor Thermal Ablation. *Physics* **2024**, *6*, 164–176. <https://doi.org/10.3390/physics6010012>

Received: 25 September 2023

Revised: 10 December 2023

Accepted: 4 January 2024

Published: 31 January 2024



Copyright: © 2024 by the author. Licensee MDPI, Basel, Switzerland. This article is an open access article distributed under the terms and conditions of the Creative Commons Attribution (CC BY) license (<https://creativecommons.org/licenses/by/4.0/>).

1. Introduction

A high rate of disorders and a stressful lifestyle in advanced society causes several dangerous diseases that increase the demand for progress in nanotechnology applications as alternative processes for treatment in order to shield and assist the shaping of people lives [1,2]. Despite many serious and epidemic diseases around the world, such as COVID-19 and avian influenza, cancer tumors represent one of the most severe illnesses and is attributed to the unexpected mutation of healthy tissue [3]. Actually, this disease induces a huge number of human deaths around the world (10 million in 2020), which require significant amounts of resources and medical care. Furthermore, cancer can impose multiple disorders and pressures on health systems, which affects the response of health care facilities, the loss of medical equipment and logistics, and the capacity of services due to insufficient resources [4]. Other than the economic effects, many researchers report that cancer causes serious debilitating events associated with the impairment of certain neurological functions and psycho-emotional behavioral disorders that require urgent treatment and ongoing rehabilitation [5]. Generally, it is quite complicate to identify the pathogenic factors of this illness that can be attributed to the impact of external carcinogens factors on the genetic system [6]. The high diversity of etiological parameters increases the risk of cell mutation, such as heavy alcohol intake, chronic inflammation, smoking, unhealthy diet, genetic factors, and environmental risk factors. Recently, it was shown that this disease statistically accounted for 1.8 million deaths in 2020, proving that lung cancer is the most harmful form of tumor worldwide due to a lack of diagnostic services, low awareness, and high infection rate (as well as factors such as smoking, pollution) [7].

Although infection by cancer is possible in any part of the lung cell, 95% of lung cancer is associated with epithelial cell and alveolar sac mutation.

Therefore, early specification and detection analyses using diagnostic process involving clinical exams, such as magnetic resonance imaging and ultrasound imaging, can guide efficient treatment and evacuation [8]. All effective strategies based on detection devices offer quantitative measurement and potential visualization for soft tissue at an n-dimension resolution without any risk of metastasis related to lung cancer. The analysis and detection phase is important for assessing and setting an appropriate process in the treatment and to avoid the dangerous impact of traditional surgery in many complicated situations associated with patient capacity and tumor structure. In recent years, cancer treatment has been a popular research topic and has received a huge amount of scientific attention worldwide in order to find more efficient new systems for different complex situations, such as hyperthermia [9]. This has resulted in a non-surgical intervention consisting of a cascading effect of heating at a defined level, contributing significantly to increases in the temperature and related agitation of water molecules that allowed a lesion in the cancer cell membrane, inhibiting its growth and proliferation [10]. Therefore, the exposed amount of heat and its derived temperature level are highly important parameters that should be manipulated adequately to avoid the full damage of tumor tissue and to protect normal tissue. In contrast, to prudently control the secondary effects during fever therapy associated with the dissipated amount of heat, a different system and design of clinical hyperthermia based on electromagnetic microwaves known as the thermal ablation technique has been developed [11]. Heat transfer induced by electromagnetic waves has applications in various fields, such as communications [12], medicine [13], food industry [14], and manufacturing [15]. However, in medicine, one of the main applications of electromagnetic wave radiation is as a heat source and as a means of delivering powerful energy to parts of the human body in applications such as in cardiology, benign prostatic hyperplasia (BPH), tumor ablation, endometrial ablation, liposuction, microwave balloon angioplasty, the microwave treatment of microbial infections, and drug delivery [16–18]. However, different parameters such as structure, size, and location of the tumor are essential for inserting one or more specific antenna into infected tissue, which can be used to improve the performance and the quality of the electromagnetic microwave effect. With the use of thermal ablation in primary healthcare clinics, a real challenge today is to achieve the best optimal treatment strategy with the appropriate target temperature and more accurate target location [19].

There is still much room for cancer treatment improvement and necessary techniques for its development using different designs—the most motivating is the ablative family, including irreversible electroporation, radiofrequency ablation (RFA), and microwave ablation (MWA) [20]. Recent clinical results discussed in many theoretical and experimental papers prove that microwave ablation (MWA) could be the future of appropriate devices for new strategy treatment and development in the field of tumor ablation [21,22]. MWA technology has several benefits compared with other systems, such as higher constant intra-tumoral temperatures, high convection profile, faster ablation times, and the capacity to treat multiple lesions using multiple probes simultaneously [23].

The study in Ref. [24] reported that the basic designs of antenna (dipole, monopole, and slot antennas) caused backward heating as a result of the unbalanced antenna structure. The study showed the performance of MWA and the efficiency of energy delivery to be dependent on the geometric form and the structure of antenna. Furthermore, different studies show that backward heating can be restrained using the new inner structure of antenna composed of a choke or sleeve, as reported in Ref. [25]. Moreover, Ref. [26] proves that slots improve the radiation properties of antennas and can be a solution for backward heating. The authors of Ref. [27] studied and analyzed the microwave ablation method using a computational approach based on finite element analysis to improve the performance of lung cancer treatment. The study [27] confirms that the treated cell area are localized around the antenna slot and tip. In Ref. [28], it is reclaimed that the structure

of the antenna can enhanced the microwave effect [23]. They also demonstrate, using numeric and experimental data, that the antenna with tri-slot design is more efficient compared to that with single-slot at a 433 MHz operating frequency. In Ref. [29] the MWA response was modeled using coaxial antenna with a single-slot at different frequencies and conclude that 2.45 GHz represents the higher frequency for therapy process. Several computational studies missed numerous parameters in the applied model, such as tissue water vaporization and shrinkage. In Ref. [30] the effect of the electrical conductivity and temperature feature on lung treatment is studied using the MWA technique. In Ref. [31] the lung tissue-containing tumor is modeled based on the finite element process and heat transfer model into porous media. They evaluated the microwave ablation of lung tumors and confirmed the proportionality trend of tumor and the power of ablation effect.

The computer modeling system represents a powerful method for treating cancerous tumor cells and offers an effective procedure for development. In preparation for surgery, theoretical models become an investigative method to understand the process inside the cancer and to optimize the best modality for a safe microwave ablation strategy. This paper reports a modeling analysis of electromagnetic (EM) wave impact in lung cell treatment using a 2D (two-dimensional) numerical model and finite element process. Different equations and approximations such as Maxwell and bioheat equations are applied to predict the distribution of the electric field and the temperature associated with the heat flux. Furthermore, different factors are analyzed, such as the fraction of necrotic tissue, SAR, and the input microwave power. In addition, a proportional–integral–derivative (PID) controller is applied to estimate the input power and the temperature which was not previously fixed.

2. Model and Methods

2.1. Model Geometry

The designed micro-coaxial slot antenna (MCA) was inserted into the cancer tumor to radiate the MW energy and to produce an extended heated zone for use in lung cancer treatment. The absorbed energy, induced by the electromagnetic field effect, was propagated into the lung cells and converted to thermal energy, which produced a dissipating heat in the lung tissue. Moreover, this process causes a rise in the tissue temperature to 50 °C or above, which can destroy cancer cells. Therefore, a programmable temperature-controlled based on the PID controller was used to control and manipulate the variable power source. This component moderates the variable power source to reach the allowable temperature rise, at which point, the necrosis occurs. Several parameters of the antenna also play crucial roles in its functionality and performance, such as the antenna frequency (2.45 GHz) and the relative permittivity of the dielectric material and catheter with values of 2.03 and 2.1, respectively.

The processes of the lung ablation-developed model principally involved MWA design and the lung tumor cells, including a MW power source and a single MCA, which is encapsulated in a plastic catheter with a diameter of 0.895 mm. In addition, the proposed form is composed of an inner conductor and a dielectric material with diameters of 0.135 mm and 0.335 mm, respectively, while an outer conductor contains a slot with a diameter of 0.460 mm, as is shown in Figure 1. As proposed in Refs. [26,32], the lung cell was considered to have a cylindrical form with height and radius values of 80 mm and 30 mm, respectively. Meanwhile, the spherical shape of the cancer cell in the lung was characterized by a radius value of 10 mm [27].

2.2. Mathematical Model

2.2.1. Heat Transfer Field

There are many models used in the literature that describe the heat transport phenomena in perfused biological tissues and organs such as Penné's bioheat model, the porous model, and the Darcy–Brinkman porous model. These are used in a wide range of applications. A review of several models available in the literature is given in Ref. [33]. In

Ref. [34], a sophisticated bioheat model based on the theory of porous media have been used. Some issues related to blood perfusion have been extensively discussed [34]. In the present study, the Penne’s model [35,36] is used.

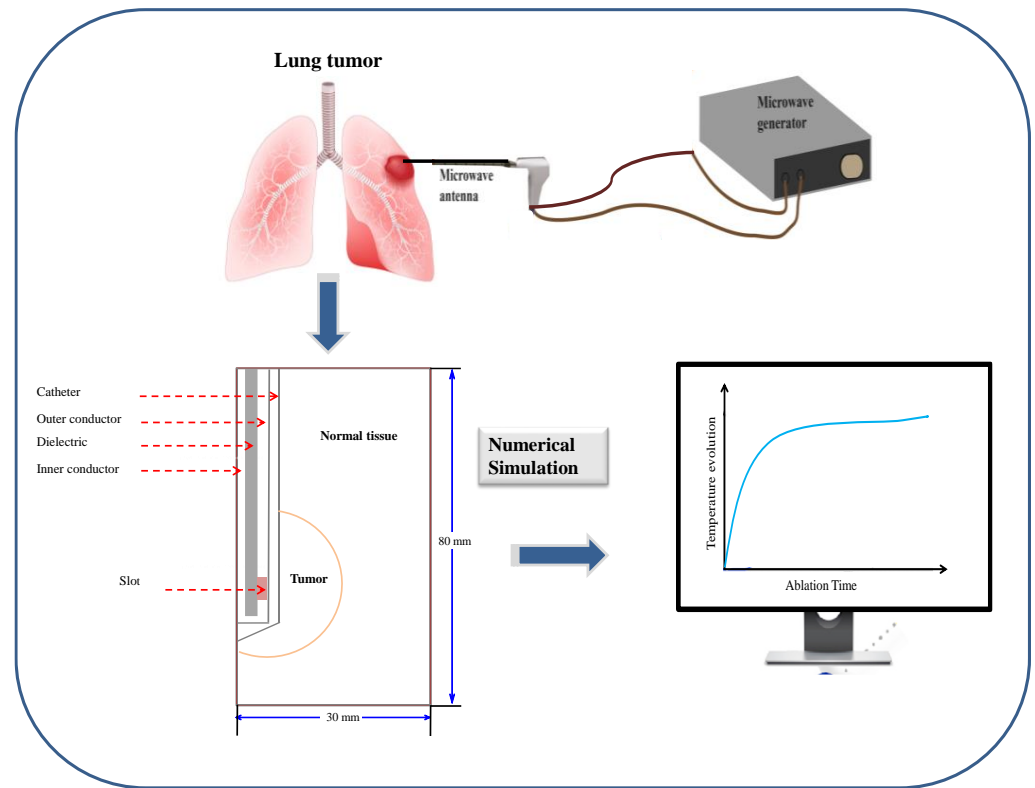


Figure 1. Schematic view of the microwave ablation system design.

The temperature profile of the lung cell was estimated to determine the relative heat using the bioheat equation as follows [37]:

$$\rho C_p \frac{\partial T}{\partial t} = \nabla(k\nabla T) + \rho_b C_b \omega_b (T_b - T) + Q_{ext} + Q_{meta}, \tag{1}$$

where T , $k = 0.39 \text{ W/m}\cdot\text{K}$, $C_p = 3886 \text{ Jkg}^{-1}\text{K}^{-1}$, and $\rho = 385 \text{ kg}\cdot\text{m}^{-3}$ denote the temperature, the thermal conductivity, the specific heat capacity, and the density of the human cell, respectively; while T_b , $\rho_b = 1060 \text{ kg}\cdot\text{m}^{-3}$, $C_b = 3639 \text{ Jkg}^{-1}\text{K}^{-1}$, and ω_b represent the temperature, the density, the specific heat capacity, and the perfusion rate of blood, respectively. t denotes the time. In this paper, the blood temperature is assumed to have a value of $T_b = 37 \text{ }^\circ\text{C}$ and the blood perfusion rate is $\omega_b = 0.0036 \text{ s}^{-1}$ [27].

The left-hand side of Equation (1) is associated with the transient term, while the first and second terms on the right-hand side of Equation (1) define the heat conduction and dissipation of the blood flow, respectively. In addition, the term Q_{meta} represents the metabolism heat source, which can be neglected in the current study, while the external heat source defined by the term Q_{ext} is related to the resistive heat of the EM wave defined by the following equation:

$$Q_{ext} = \frac{\sigma}{2} \|E_0\|^2, \tag{2}$$

where E_0 represents the electric field amplitude created by the inserted MCA and σ represent the electric conductivity of the lung tissue (in S/m). The factor $\frac{1}{2}$ should be taken into account in Equation (2) in order to take into account the averaging of the data in the sinusoidal mode.

This applied electromagnetic wave energy absorbed into the lung tissue produced an internal heat generation leads to an increase in lung temperature. This process is basically

dependent on the external energy provided by the unit mass of the tissue, which can be defined as the SAR [38]:

$$SAR = \frac{Q_{ext}}{\rho} = \frac{\sigma}{2\rho} \|E_0\|^2. \tag{3}$$

In this study, the thermophysical [39] and dielectric [40] properties for both lung tissue and tumor are considered to be temperature-independent.

2.2.2. Electromagnetic Field

MW ablation system represents an important technique for producing a large enough ablation zone and a rise in the temperature in the tumor tissue in order to destroy the cancer cells. For this reason, an MCA was inserted into the lung cell to generate the input MW power and create an electromagnetic wave responsible for killing the tumor. It was uncovered that the antenna generates an axisymmetric wave modes propagation (i.e., the magnetic and electric field components of the wave each is independent of the azimuthal angle (ϕ)) and characterized by transverse magnetic fields. In this context, the propagation of the magnetic field has only an azimuthal direction and follows the relationship,

$$H = H_\phi e_\phi, \tag{4}$$

where e_ϕ represents the unit vector, which can be defined by cylindrical coordinates:

$$H_\phi = H_0(r, z) e^{j(\omega t - kz)}, \tag{5}$$

where ω represents the angular frequency of the wave and k is the wave number.

The wave equation is defined by the expression as follows:

$$\nabla \times \left(\left(\epsilon_r - \frac{j\sigma}{\omega\epsilon_0} \right)^{-1} \nabla \times \vec{H}_\phi \right) - \mu_r \frac{\omega^2}{c^2} \vec{H}_\phi = 0, \tag{6}$$

where $\epsilon_0 = 8.8542 \times 10^{-12}$ F/m represents the vacuum permittivity and c denotes the speed of light. The configuration of the electric field in cylindrical symmetry is represented using the following coordinate system [41,42]:

$$\begin{cases} E_r = -\frac{1}{\sigma + j\omega\epsilon_0\epsilon_r} \frac{\partial H_\phi}{\partial z}, \\ E_\phi = 0, \\ E_z = \frac{1}{\sigma + j\omega\epsilon_0\epsilon_r} \frac{1}{r} \frac{\partial(rH_\phi)}{\partial r}. \end{cases} \tag{7}$$

2.2.3. Thermal Damage Equation

The method of assessing human tissue destruction using thermal damage system has been quantified and described by employing a first-order Arrhenius rate expression [43]:

$$\alpha(t) = \int_0^t A e^{-\frac{E_a}{RT}} dt, \tag{8}$$

where A (in 1/s) represents the frequency parameters, T represents the absolute temperature, R denotes the gas constant, E_a (in J/mol) is the activation energy, leading to irreversible thermal damage depending upon the tissue type. α denotes the degree of tissue damage and estimates the variation in the stored energy amount in the body over time. In this study, the aforementioned quantities refer to the values used: $A = 1.18 \times 10^{44}$ 1/s, $R = 8.314$ J/mol·K, and $E_a = 3.02 \times 10^5$ J/mol [44].

Then, the fraction θ_d of tissue necrosis is predicted using the parameter α as follows [45]:

$$\theta_d = 1 - e^{-\alpha}. \tag{9}$$

2.2.4. Temperature-Controlled MWA

During MWA therapy, the accuracy of temperature represents significant parameters in clinical treatment that should be controlled in order to eradicate any adverse impacts and improve efficiency. Actually, the control of temperature behavior should be monitored in real-time to minimize the destruction rate of the surrounding biologic tissues. In the present system, to keep and track the target tip temperature (T_{tip}) when it is less than the pre-set temperature (T_{set}) during MWA, the input MW power source is evaluated using a temperature-controlled program modeled using the incorporate the PID controller, as shown in Figure 2.

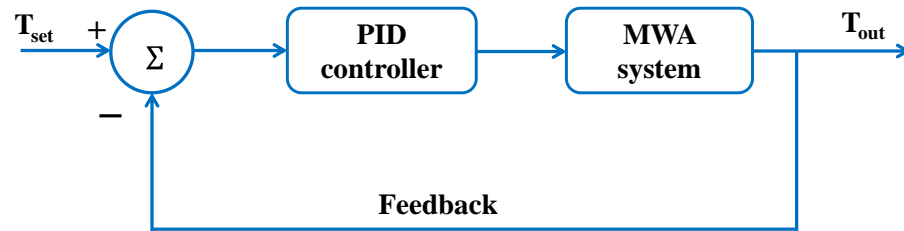


Figure 2. The MWA process and PID controller systems used in the present study. See text for details.

The input MW power is estimated as

$$P_{in}(t) = K_P(T_{set} - T_{tip}) + K_I \int_0^t (T_{set} - T_{tip})dt + K_D \frac{\partial}{\partial t} (T_{set} - T_{tip}), \quad (10)$$

where K_I , K_P , and K_D are the integral, proportional, and derivative coefficients, respectively. Here, it is assumed that the coefficients take the values of $K_P = 0.17$, $K_I = 0.0045$, and $K_D = 0$ [46] and that the pre-set temperature, T_{set} , varies within the range of 60 °C to 90 °C.

Many experimental and theoretical studies have been performed to analyze the efficacy of temperature-controlled radiofrequency ablation (RFA) in different tissues using PID controllers [43,44]. A complete PID controller with a constant $K_D \neq 0$ is planned to be investigated in a future work; in particular, the effect of K_D will be analyzed.

In Ref. [47], a study was carried out to provide comprehensive information on the relationship between RF waveforms and the thermodynamic response of the tissue with the consideration of four different types of RF waveforms (half-sine, half-square, half-exponential, and damped-sine) to maximize the amount of tumor tissue removed while maintaining the advantages of RF ablation.

In Ref. [48], the authors studied the differences between continuous and short-pulse mode microwave ablation (MWA). Their computational models predicted that the characteristics of the coagulation zone created by continuous and pulsed MWA show no significant differences from ex vivo experiments and computer simulations.

2.3. Boundary Conditions

During the numerical simulation, boundaries conditions that are attributed to the electromagnetic field propagation and the related heat transfer equation were utilized.

2.3.1. Boundary Conditions for Heat Transfer Field Analysis

As the heat distribution analysis is considered in the lung organ only, the appropriate boundary conditions implicated in the heat transfer equations can be described as follows:

- i The surrounding healthy lung tissue is considered as an insulation condition $n \cdot (k \nabla T) = 0$.
- ii An axial symmetry boundary condition at $r = 0$ is adopted.
- iii The presence of continuous heat flux through the cancer and the lung tissue is assumed, which can be expressed by $n \cdot (k_{liver} \nabla T_{liver}) = n \cdot (k_{tumor} \nabla T_{tumor})$.

A constant temperature with a value of $T(t = 0, r, z) = 37$ °C is assumed for the initial resolution of the heat transfer calculation.

2.3.2. Boundary Conditions for Electromagnetic Field Analysis

MCA was inserted into the lung tissue to deliver the EM energy in MW therapy, which is also governed by inlet power density. For this reason, one should include an important variable in the analyses related to the input MW power, namely P_{in} , which is estimated by the PID controller. Furthermore:

- i In this model, it is assumed that the z -axis represents a symmetry axis: $E_r(t, r = 0, z)$ and $\frac{\partial E_z}{\partial r}(t, r = 0, z)$.
- ii The scattering boundary condition is applied along the outer side of the lung ($z = 0$ or $z = 80$ mm or $r = 30$ m).
- iii The walls of the antenna with the values $r = 0.47$ mm or $r = 0.135$ mm or $r = 0.594$ mm are computed as perfect metal conductors: $n \cdot E = 0$.
- iv At the tumor–lung interface, the continuity behavior of the tangential component of the electric field \vec{E} is imposed by $n \wedge (E_{liver} - E_{tumor}) = 0$.

2.4. Numerical Method and Verification of Simulation Model

The computational model applied in this analysis is implemented to explain MWA system and its potential effect in tumor lung tissues treatment with the respect to different parameters and factor such as energy, temperature, and power. The modeling is carried out using the Galerkin finite element approach [49]. In addition to the preliminary results, the computing scheme using 5813 triangular geometric pieces across the 2D domain, containing the optimized reaction surface and electrode components, are depicted in Figure 3a. To demonstrate that convergence has occurred and that the estimated values are independent of mesh size, Figure 3b shows the temperature within tissue for multiple mesh grids, namely 5813, 10,928, 14,264, and 17,664 elements. The resulting versions with varying element counts are quite similar.

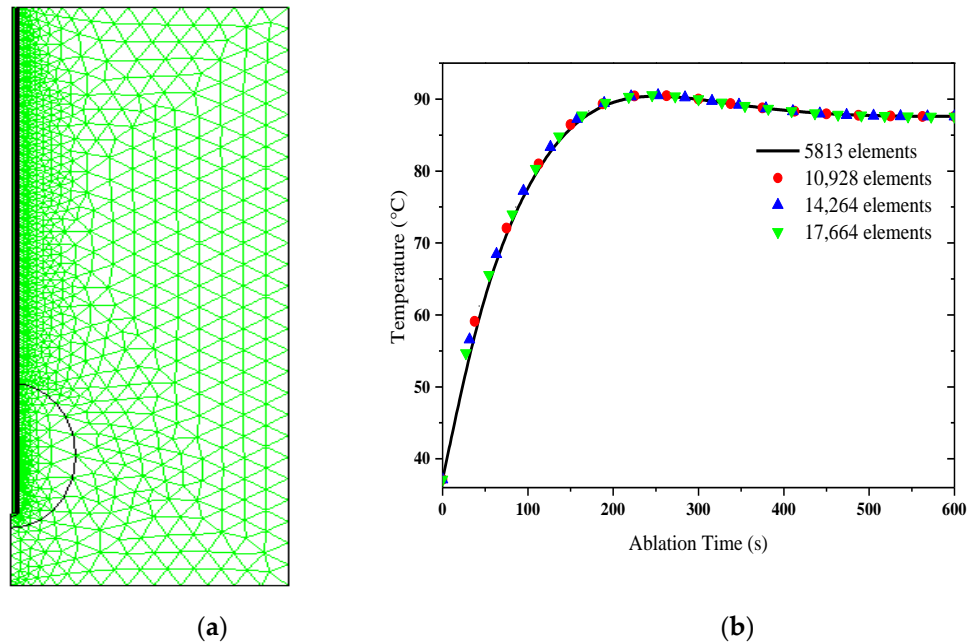


Figure 3. (a) Representation of the two-dimensional domain meshing. (b) Temporal evolution of the temperature during thermal ablation for several mesh grids.

The adopted mesh and time-step allow to track the space and time evolutions of the temperature with an acceptable precision.

The main output data predicted from the bioheat model were compared to the experimental profiles collected and analyzed in Ref. [50] in order to check the accuracy of the mathematical model.

During the MWA process, the numerical validation of temperature distribution in the lung tissue is available in our previous study [42].

One can find that the discrepancies between the theoretical results obtained here using the present model and the experimental data curves achieved in Ref. [50] are quite close, that proves that the limited differences method is satisfactory enough. This proves also the reliability of the model considered here.

3. Results and Discussion

The propagation of the thermal energy during the heat therapy induces an increase in the temperature into the lung tissue, which may exceed 50 °C and consequently yield an excessive distribution of the energy into the whole tissue [51]. However, the transplanted micro-antenna in the tumor heats up the cancer cell directly. Therefore, the best cancer therapy considers the dose of thermal energy amount distributed only in the cancer tissue in order to conserve the healthy cells. One of the challenges faced is the need to evacuate the MW energy generated by the antenna to avoid the risk of the healthy cell damage related to overheating when the temperature approaches 100 °C. As a result, it is essential to control the applied temperature within the cancer cell which should not exceed a certain level. That said, the purpose of this research is to study the electro-thermal behavior of MWA using numerical simulations. Taking into account the heating rate during the ablation treatment process, the temperature data acquired at each control point provide precious information to develop a most useful tool for cancer treatment. As a result, some critical points in the system to be analyzed in order to control the temperature distribution related to the antenna and cancer frontier.

3.1. Effect of Target Tip Temperature on the Applied Input Power during MWA

As explained above, an accurate knowledge of the target tip temperature is essential for the present study. Therefore, the input MWA needs to be estimated. There are important points that should be considered in regard to the controlled of temperature during MWA, namely P_1 ($r = 0.895$ mm, $z = 18$ mm), the limit of the antenna, and P_2 ($r = 7$ mm, $z = 18$ mm), the limit of the tumor. Figure 4 illustrates the time dependency of the input power data for several target tip temperature values at the two positions, P_1 and P_2 . One can see that the input microwave power rises with the increase of the temperature in the range of 60 °C to 90 °C. Actually, the heat propagation in the biological tissue induces a variable feature of the input microwave power, which tends gradually toward a uniform value affected by the target tip temperature. For a particular target tip temperature, the estimated value of maximum power exhibits a significant change between the two points in terms of temperature control.

3.2. Effect of Target Tip Temperature on Temperature during MWA

The MWA process has many benefits, particularly compared to other ablation techniques, and represents the most effective way to treat cancer cells without bringing whatever damage to healthy cells through overheating. To predict and moderate the MWA-technique efficiency and to control the applied heat of thermal doses, the temperature profile should be taken into consideration. Significant research efforts have been conducted in order to improve the required temperature in this process and to accurately predict the outcomes of thermal energy [43,44,50]. Generally, the amount of thermal energy applied in cancer therapy is attributed to different critical parameters, such as the effect of tumor cell temperature, tissue temperature, and the electrical conductivity during tumor ablation application.

Figure 5 shows the time dependence of the ablation temperature under several target temperatures at points P_1 and P_2 . As one would expect, the variations in temperature data as a function of the target temperature at P_1 and P_2 , accounting for computational models, indicate a linear behavior attributed to the source term and the small duration of ablation. One notices quite a fast initial response at each temperature accompanied by a rapid increase, which can be explained using the properties of the cancer cell and

the surrounding tissue. Further increase in the time yields a visible asymptotic value of the obtained data related to the temperature and the contribution of the blood effect. In addition, a dynamic response raises the blood flow and its perfusion, which imposes a counterbalance of the external factor. The numerical predictions also show divergences in the features and prove the effect and the contribution of tissue properties on the temperature during MWA. Moreover, the position P_1 requires less time in the heating period to reach saturation compared to the position P_2 what confirms that the optimal duration depends on the position.

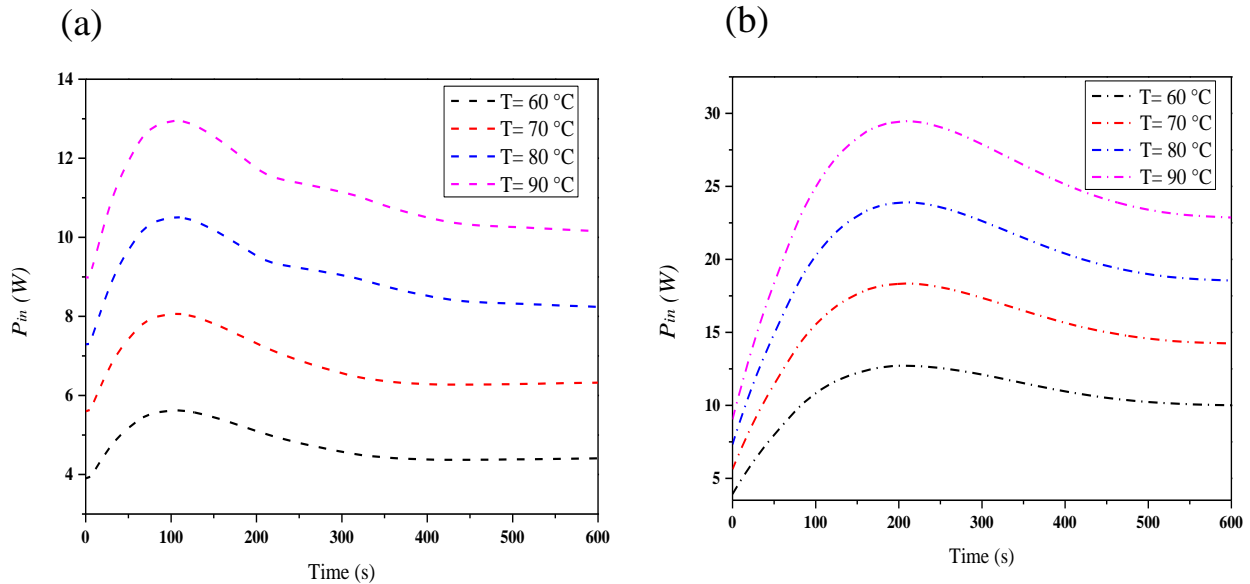


Figure 4. Effect of the target tip temperature T ($60\text{ }^{\circ}\text{C}$ to $90\text{ }^{\circ}\text{C}$) on PID-controlled input microwave power, P_{in} (see Equation (10)), at two measurement points (a) P_1 (the limit in the antenna) and (b) P_2 (the limit in the tumor).

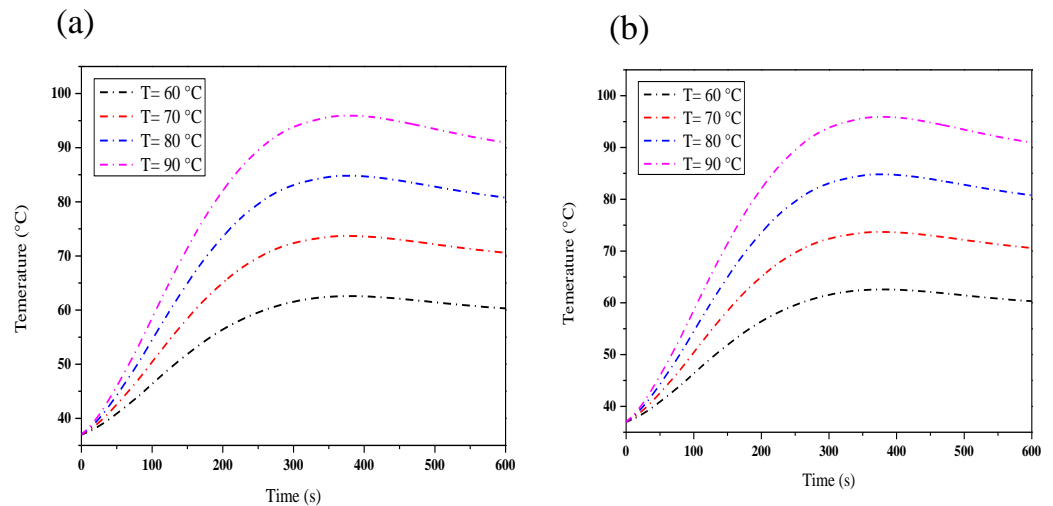


Figure 5. Temporal evolution of temperature at the measurement points (a) P_1 and (b) P_2 for different tip temperatures as indicated.

3.3. Effect of Target Tip Temperature on SAR

The electromagnetic wave absorption of the human body has been extensively investigated in order to determine its response on the MWA process using SAR (in Wkg^{-1}). This parameter represents important information that serves to quantify the effect of the EM waves on the biological tissues and can be directly estimated from the ratio of absorbed heat energy and tissue density. Figure 6 shows the calculations of the

SAR as a function of the insertion depth, z , and the temperature at the two positions ($r_1 = 0.895$ mm and $r_2 = 7$ mm) with several target tip temperatures. It should be noted that in Figure 6a, the two peaks occur. The first peak is situated in the vicinity of the slot antenna whereas the second peak is situated near the bottom of the antenna. Moreover, one can see that the SAR curve performs a similar behavior for all measured temperatures, the feature which can be explained on the basis of the thermal activation energies framework. To note is that the level of the SAR rises slightly along the axis parallel to the MCA and achieves its highest values near the slot, consistent with earlier results [41]. Finally, a hyperbolic decrease in the behavior of the SAR curve can be observed with the increase in the antenna insertion into human body at the depth z . This process confirms that the SAR distribution depends on the target location temperature. At high temperatures, the SAR values inside the lung tissue were obtained to be larger than those at the surface indicating that the high capacity of the energy absorption by the human body is related to the depth z and the temperature value.

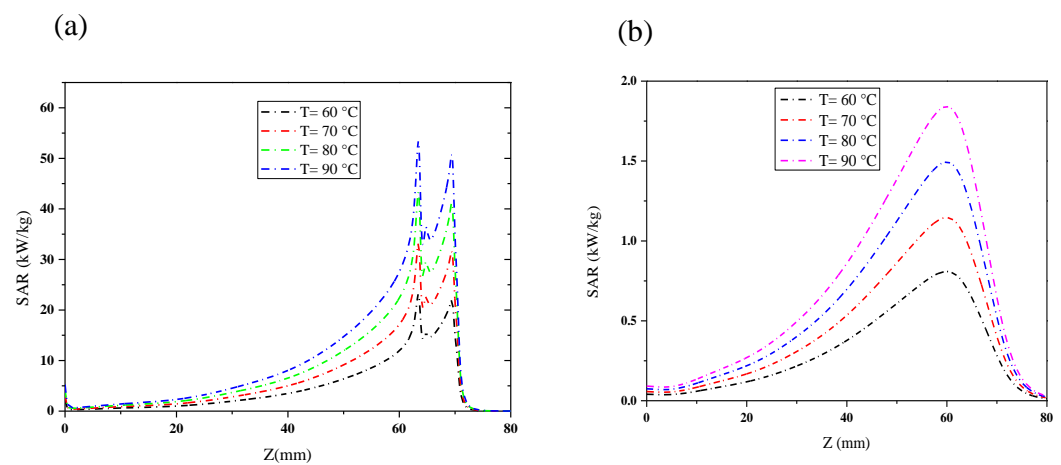


Figure 6. Effect of the target tip temperature T on the SAR (see Equation (3)) along the z -axis at $t = 600$ s at the measurement points (a) P_1 and (b) P_2 .

3.4. Effect of Target Tip Temperature on the Fraction of Necrotic Tissue

Figure 7 shows the MWA time dependence of the simulated necrotic tissue data under several different target tip temperatures. As expected, when increasing the MWA period, one can see that at each temperature, the theoretical curves of damage tissue rise quite slowly and reach a saturation value associated with the required time for complete cancer destruction. These findings suggest that temperature has an important effect on the treatment of tumors and prove that the resulting damage is influenced by the treated position due to the physical properties of the human tissue. Another factor to take into consideration regarding the ablation process is related to the delay in response for a few seconds before the damage, which can be associated with the tissue nature and the starting target temperature level. In addition, the increase in the target tip temperature ultimately leads to a decrease in the initiation–damage time symptoms, and its highest rate corresponds to the earliest response onset. This phenomenon is attributed to the contribution of the target tip temperatures and applied input voltage as the two proportional factors responsible for the necrosis initiation time. On the other hand, the damage at P_1 tended to occur earlier compared to that at P_2 what implies that the position and tissue properties indeed play crucial roles in the cancer tumor destruction. It is worth noting that the analysis with the present parameters allows the setting of an efficient ablation period in the absence of the destruction of any healthy cells.

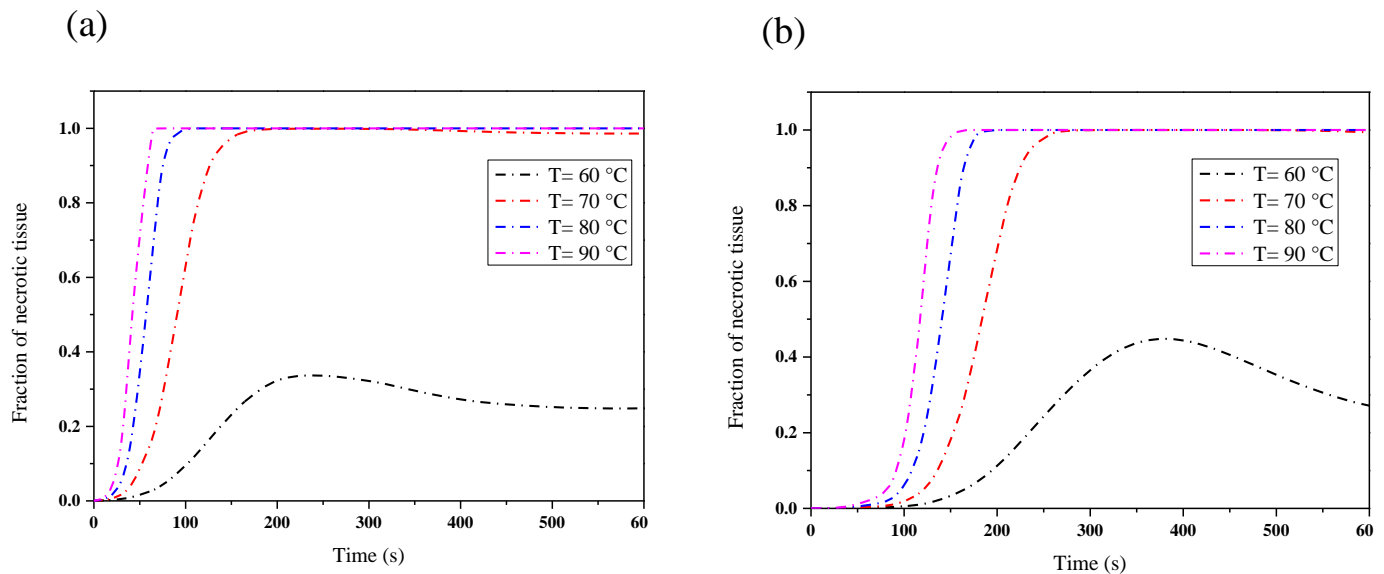


Figure 7. Temporal evolution of the fraction of necrotic tissue during thermal ablation at the measurement points (a) P_1 and (b) P_2 at different tip temperatures as indicated.

4. Conclusions

Numerical modeling and its simulation were applied in this investigation to analyze and quantify different critical parameters in order to find the most significant impact of the MWA procedure in tumor cancer treatment, which depends on the treatment position. The application of the EM wave across the lung tumors affords a conductive and convective heat transfer used in the therapy system. Here, the simulation and theoretical calculations using the finite element method were performed to supply the a priori information required for safe and reliable treatment via a thermo-electrical interaction system. Different critical parameters were analyzed and studied in order to evaluate and then improve the efficiency of the MWA process, in terms of, e.g., the number of necrotic tumor cells, the temperature distribution profile, the SAR, and the absorbed microwave power density. The biophysical and thermo-electrical properties of the tissue demonstrated different features for the analyzed parameters. Moreover, the electromagnetic wave was found to be influenced by the treatment position (inside/on surface) and the intrinsic behavior of the tissue were shown to be related to the temperature and the blood flow. The study shows that the intrinsic properties of each position and the required time for treatment should be known in order to achieve the optimal operation and high performance of MWA. As well the target temperature position and the temperature value were shown to affect SAR behavior.

Let us note that, in the presented investigation, the tumor was considered a sphere with a 10 mm radius. The effects of the shape and size of a tumor to be investigated in further studies. As well, the future research on the topic considered include, for example, a consideration applying other bioheat models, use of a more complete PID controller, investigations of 2D and 3D temperature distributions.

Funding: This research received no external funding.

Data Availability Statement: The data presented in this study are available on request from the author.

Conflicts of Interest: The author declares no conflicts of interest.

References

- Zhu, Q.; Chua, M.H.; Ong, P.J.; Cheng Lee, J.J.; Le Osmund Chin, K.; Wang, S.; Kai, D.; Ji, R.; Kong, J.; Dong, Z.; et al. Recent advances in nanotechnology-based functional coatings for the built environment. *Mater. Today Adv.* **2022**, *15*, 100270. [[CrossRef](#)]
- An, C.; Sun, C.; Li, N.; Huang, B.; Jiang, J.; Shen, Y.; Wang, C.; Zhao, X.; Cui, B.; Wang, C.; et al. Nanomaterials and nanotechnology for the delivery of agrochemicals: Strategies towards sustainable agriculture. *J. Nanobiotechnol.* **2022**, *20*, 11. [[CrossRef](#)]

3. Subramaniyan, V.; Fuloria, S.; Gupta, G.; Kumar, D.H.; Sekar, M.; Sathasivam, K.V.; Sudhakar, K.; Alharbi, K.S.; Al-Malki, W.H.; Afzal, O.; et al. A review on epidermal growth factor receptor's role in breast and non-small cell lung cancer. *Chem.-Biol. Interact.* **2022**, *351*, 109735. [[CrossRef](#)] [[PubMed](#)]
4. Roy, N.; Villavisanis, D.F.; Taub, P.J. Mitigating financial toxicity in breast cancer from diagnosis to treatment and reconstruction. *Clin. Breast Cancer* **2023**, *23*, e32–e36. [[CrossRef](#)] [[PubMed](#)]
5. Beaver, S.K.; Mesa-Torres, N.; Pey, A.L.; Timson, D.J. NQO1: A target for the treatment of cancer and neurological diseases, and a model to understand loss of function disease mechanisms. *Biochim. Biophys. Acta Proteins Proteom.* **2019**, *1867*, 663–676. [[CrossRef](#)]
6. Parsa, N. Environmental factors inducing human cancers. *Iran. J. Public Health* **2012**, *41*, 1–9. Available online: <https://ijph.tums.ac.ir/index.php/ijph/article/view/2480> (accessed on 3 January 2024)
7. George, J.; Lim, J.S.; Jang, S.J.; Cun, Y.; Ozretić, L.; Kong, G.; Leenders, F.; Lu, X.; Fernández-Cuesta, L.; Bosco, G.; et al. Comprehensive genomic profiles of small cell lung cancer. *Nature* **2015**, *524*, 47–53. [[CrossRef](#)]
8. Donato, S.; Brombal, L.; Arana Peña, L.M.; Arfelli, F.; Contillo, A.; Delogu, P.; Di Lillo, F.; Di Trapani, V.; Fanti, V.; Longo, R.; et al. Optimization of a customized simultaneous algebraic reconstruction technique algorithm for phase-contrast breast computed tomography. *Phys. Med. Biol.* **2022**, *67*, 95012. [[CrossRef](#)]
9. Dharmaiyah, S.; Zeng, J.; Rao, V.S.; Zi, O.; Ma, T.; Yu, K.; Bhatt, H.; Shah, C.; Godley, A.; Xia, P.; et al. Clinical and dosimetric evaluation of recurrent breast cancer patients treated with hyperthermia and radiation. *Int. J. Hyperth.* **2019**, *36*, 986–992. [[CrossRef](#)]
10. Oršolić, N.; Odeh, D.; Jembrek, M.J.; Knežević, J.; Kučan, D. Interactions between cisplatin and quercetin at physiological and hyperthermic conditions on cancer cells in vitro and in vivo. *Molecules* **2020**, *25*, 3271. [[CrossRef](#)]
11. Bailey, C.W.; Sydnor, M.K., Jr. Current state of tumor ablation therapies. *Dig. Dis. Sci.* **2019**, *64*, 951–958. [[CrossRef](#)] [[PubMed](#)]
12. Li, M.; Zhu, N. Recent advances in microwave photonics. *Front. Optoelectron.* **2016**, *9*, 160–185. [[CrossRef](#)]
13. Rosen, A.; Stuchly, M.A.; Vorst, A.V. Applications of RF/microwaves in medicine. *IEEE Trans. Microw. Theory Tech.* **2002**, *50*, 963–974. [[CrossRef](#)]
14. Chandrasekaran, S.; Ramanathan, S.; Basak, T. Microwave food processing—A review. *Food Res. Int.* **2013**, *52*, 243–261. [[CrossRef](#)]
15. Kim, J.; Mun, S.C.; Ko, H.-U.; Kim, K.-B.; Khondoker, M.A.H.; Zhai, L. Review of microwave assisted manufacturing technologies. *Int. J. Precis. Eng. Manuf.* **2012**, *13*, 2263–2272. [[CrossRef](#)]
16. Vander Vorst, A.; Rosen, A.; Kotsuka, Y. *RF/Microwave Interaction with Biological Tissues*; John Wiley & Sons, Inc.: Hoboken, NJ, USA, 2006. [[CrossRef](#)]
17. Parés, C.; Berjano, E.; González-Suárez, A. Effect of intracardiac blood flow pulsatility during radiofrequency cardiac ablation: Computer modeling study. *Int. J. Hyperth.* **2021**, *38*, 316–325. [[CrossRef](#)] [[PubMed](#)]
18. Adabbo, G.; Andreozzi, A.; Iasiello, M.; Netti, P.A.; Vanoli, G.P. A 3D numerical model of controlled drug delivery to solid tumor by means of mild microwave hyperthermia-activated thermo-sensitive liposomes. *Int. J. Therm. Sci.* **2023**, *193*, 108528. [[CrossRef](#)]
19. Testoni, S.G.G.; Healey, A.J.; Dietrich, C.F.; Arcidiacono, P.G. Systematic review of endoscopy ultrasound-guided thermal ablation treatment for pancreatic cancer. *Endosc. Ultrasound* **2020**, *9*, 83–100. [[CrossRef](#)]
20. Wada, T.; Sugimoto, K.; Sakamaki, K.; Takahashi, H.; Kakegawa, T.; Tomita, Y.; Abe, M.; Yoshimasu, Y.; Takeuchi, H.; Itoi, T. Comparisons of radiofrequency ablation, microwave ablation, and irreversible electroporation by using propensity score analysis for early stage hepatocellular carcinoma. *Cancers* **2023**, *15*, 732. [[CrossRef](#)]
21. Cornelis, F.H.; Marcelin, C.; Bernhard, J.C. Microwave ablation of renal tumors: A narrative review of technical considerations and clinical results. *Diagn. Interv. Imaging* **2017**, *98*, 287–297. [[CrossRef](#)]
22. Prakash, P. Theoretical modeling for hepatic microwave ablation. *Open Biomed. Eng. J.* **2010**, *4*, 27–38. [[CrossRef](#)]
23. Floridi, C.; De Bernardi, I.; Fontana, F.; Muollo, A.; Ierardi, A.M.; Agostini, A.; Fonio, P.; Squillaci, E.; Brunese, L.; Fugazzola, C.; et al. Microwave ablation of renal tumors: State of the art and development trends. *Radiol. Medica* **2014**, *119*, 533–540. [[CrossRef](#)] [[PubMed](#)]
24. Huang, H.; Zhang, L.; Moser, M.A.J.; Zhang, W.; Zhang, B. A review of antenna designs for percutaneous microwave ablation. *Phys. Medica* **2021**, *84*, 254–264. [[CrossRef](#)] [[PubMed](#)]
25. Wakaki, T.; Michiyama, T.; Kuwano, S. A new interstitial choke embedded antenna for microwave ablation. *IEICE Commun. Express* **2017**, *6*, 435–438. [[CrossRef](#)]
26. Wang, T.; Zhao, G.; Qiu, B. Theoretical evaluation of the treatment effectiveness of a novel coaxial multi-slot antenna for conformal microwave ablation of tumors. *Int. J. Heat Mass Transf.* **2015**, *90*, 81–91. [[CrossRef](#)]
27. Radmilović-Radjenović, M.; Sabo, M.; Prnova, M.; Šoltes, L.; Radjenović, B. Finite element analysis of the microwave ablation method for enhanced lung cancer treatment. *Cancers* **2021**, *13*, 3500. [[CrossRef](#)] [[PubMed](#)]
28. Jiang, Y.; Zhao, J.; Li, W.; Yang, Y.; Liu, J.; Qian, Z. A coaxial slot antenna with frequency of 433 MHz for microwave ablation therapies: Design, simulation, and experimental research. *Med. Biol. Eng. Comput.* **2017**, *55*, 2027–2036. [[CrossRef](#)] [[PubMed](#)]
29. Curto, S.; Taj-Eldin, M.; Fairchild, D.; Prakash, P. Microwave ablation at 915 MHz vs 2.45 GHz: A theoretical and experimental investigation. *Med. Phys.* **2015**, *42*, 6152–6161. [[CrossRef](#)]
30. Tian, Z.; Cheng, Y.; Dong, T.; Gao, X.; Nan, Q. Numerical study for lung microwave ablation in different thermal and electrical properties. In *World Congress on Medical Physics and Biomedical Engineering 2018. June 3–8, 2018, Prague, Czech Republic (Vol. 1)*; Lhotska, L., Sukupova, L., Lacković, I., Ibbot, G.S., Eds.; Springer Nature Singapore Pte Ltd.: Singapore, 2019; pp. 563–566. [[CrossRef](#)]

31. Mai, X.; Wu, N.; Nan, Q.; Bi, S. Simulation study of microwave ablation of porous lung tissue. *Appl. Sci.* **2023**, *13*, 625. [[CrossRef](#)]
32. Rattanadecho, P.; Keangin, P. Numerical study of heat transfer and blood flow in two-layered porous liver tissue during microwave ablation process using single and double slot antenna. *Int. J. Heat Mass Transf.* **2013**, *58*, 457–470. [[CrossRef](#)]
33. Andreozzi, A.; Brunese, L.; Iasiello, M.; Tucci, C.; Vanoli, G.P. Modeling heat transfer in tumors: A review of thermal therapies. *Ann. Biomed. Eng.* **2019**, *47*, 676–693. [[CrossRef](#)]
34. Nakayama, A.; Kuwahara, F. A general bioheat transfer model based on the theory of porous media. *Int. J. Heat Mass Transf.* **2008**, *51*, 3190–3199. [[CrossRef](#)]
35. Selmi, M.; Iqbal, A.; Smida, A.; Waly, M.I.; Belmabrouk, H. Modeling of heat transfer distribution in tumor breast cancer during microwave ablation therapy. *Microw. Opt. Technol. Lett.* **2022**, *64*, 1364–1375. [[CrossRef](#)]
36. Selmi, M.; Bajahzar, A.; Belmabrouk, H. Effects of target temperature on thermal damage during temperature-controlled MWA of liver tumor. *Case Stud. Therm. Eng.* **2022**, *31*, 101821. [[CrossRef](#)]
37. Pennes, H.H. Analysis of tissue and arterial blood temperatures in the resting human forearm. 1948. *J. Appl. Physiol.* **1998**, *85*, 5–34. [[CrossRef](#)]
38. Krishnan, R.; Christ, J. An investigation using specific absorption rate analysis to diagnose early-stage breast tumor using UWB antenna. *Curr. Med. Imaging* **2021**, *17*, 1425–1431. [[CrossRef](#)] [[PubMed](#)]
39. Bianchi, L.; Cavarzan, F.; Ciampitti, L.; Cremonesi, M.; Grilli, F.; Saccomandi, P. Thermophysical and mechanical properties of biological tissues as a function of temperature: A systematic literature review. *Int. J. Hyperth.* **2022**, *39*, 297–340. [[CrossRef](#)] [[PubMed](#)]
40. Wardhana, G.; Almeida, J.P.; Abayazid, M.; Fütterer, J.J. Development of a thermal model for irreversible electroporation: An approach to estimate and optimize the IRE protocols. *Int. J. Comput. Assist. Radiol. Surg.* **2021**, *16*, 1325–1334. [[CrossRef](#)]
41. Keangin, P.; Rattanadecho, P.; Wessapan, T. An analysis of heat transfer in liver tissue during microwave ablation using single and double slot antenna. *Int. Commun. Heat Mass Transf.* **2011**, *38*, 757–766. [[CrossRef](#)]
42. Selmi, M.; Bin Dukhyil, A.A.; Belmabrouk, H. Numerical analysis of human cancer therapy using microwave ablation. *Appl. Sci.* **2020**, *10*, 211. [[CrossRef](#)]
43. Singh, S.; Repaka, R. Effect of different breast density compositions on thermal damage of breast tumor during radiofrequency ablation. *Appl. Therm. Eng.* **2017**, *125*, 443–451. [[CrossRef](#)]
44. Singh, S.; Repaka, R. Numerical investigation of convective cooling in minimizing skin burns during radiofrequency ablation of breast tumor. *Sādhanā* **2018**, *43*, 90. [[CrossRef](#)]
45. Jasiński, M. Investigation of tissue thermal damage process with application of direct sensitivity method. *Mol. Cell. Biomech.* **2013**, *10*, 183–199. [[CrossRef](#)]
46. Wang, X.R.; Gao, H.J.; Wu, S.C.; Jiang, T.; Zhou, Z.H.; Bai, Y.P. Numerical evaluation of ablation zone under different tip temperatures during radiofrequency ablation. *Math. Biosci. Eng.* **2019**, *16*, 2514–2531. [[CrossRef](#)] [[PubMed](#)]
47. Lim, D.; Namgung, B.; Woo, D.G.; Choi, J.S.; Kim, H.S.; Tack, G.R. Effect of input waveform pattern and large blood vessel existence on destruction of liver tumor using radiofrequency ablation: Finite element analysis. *J. Biomech. Eng.* **2010**, *132*, 61003. [[CrossRef](#)] [[PubMed](#)]
48. Radosevic, A.; Prieto, D.; Burdío, F.; Berjano, E.; Prakash, P.; Trujillo, M. Short pulsed microwave ablation: Computer modeling and ex vivo experiments. *Int. J. Hyperth.* **2021**, *38*, 409–420. [[CrossRef](#)]
49. Chen, Z. *Finite Element Methods and Their Applications*; Springer: Berlin/Heidelberg, Germany, 2005. [[CrossRef](#)]
50. Yang, D.; Converse, M.C.; Mahvi, D.M.; Webster, J.G. Expanding the bioheat equation to include tissue internal water evaporation during heating. *IEEE Trans. Bio-Med. Eng.* **2007**, *54*, 1382–1388. [[CrossRef](#)]
51. Jamil, M.; Ng, E.Y. Quantification of the effect of electrical and thermal parameters on radiofrequency ablation for concentric tumour model of different sizes. *J. Therm. Biol.* **2015**, *51*, 23–32. [[CrossRef](#)]

Disclaimer/Publisher’s Note: The statements, opinions and data contained in all publications are solely those of the individual author(s) and contributor(s) and not of MDPI and/or the editor(s). MDPI and/or the editor(s) disclaim responsibility for any injury to people or property resulting from any ideas, methods, instructions or products referred to in the content.